Alternative outlets for sustaining photosynthetic electron transport during dark-to-light transitions

Shai Saroussi[a,1], Devin A. J. Karns[b], Dylan C. Thomas[b], Clayton Bloszies[c], Oliver Fiehn[c], Matthew C. Posewitz[b], and Arthur R. Grossman[a,1]

[a]Department of Plant Biology, Carnegie Institution for Science, Stanford, CA 94305; [b]Department of Chemistry and Geochemistry, Colorado School of Mines, Golden, CO 80401; and [c]West Coast Metabolomics Center, University of California, Davis, CA 95616

Environmental stresses dramatically impact the balance between the production of photosynthetically derived energetic electrons and Calvin–Benson–Bassham cycle (CBBC) activity; an imbalance promotes accumulation of reactive oxygen species and causes cell damage. Hence, photosynthetic organisms have developed several strategies to route electrons toward alternative outlets that allow for storage or harmless dissipation of their energy. In this work, we explore the activities of three essential outlets associated with *Chlamydomonas reinhardtii* photosynthetic electron transport: (*i*) reduction of O_2 to H_2O through flavodiiron proteins (FLVs) and (*ii*) plastid terminal oxidases (PTOX) and (*iii*) the synthesis of starch. Real-time measurements of O_2 exchange have demonstrated that FLVs immediately engage during dark-to-light transitions, allowing electron transport when the CBBC is not fully activated. Under these conditions, we quantified maximal FLV activity and its overall capacity to direct photosynthetic electrons toward O_2 reduction. However, when starch synthesis is compromised, a greater proportion of the electrons is directed toward O_2 reduction through both the FLVs and PTOX, suggesting an important role for starch synthesis in priming/regulating CBBC and electron transport. Moreover, partitioning energized electrons between sustainable (starch; energetic electrons are recaptured) and nonsustainable (H_2O; energetic electrons are not recaptured) outlets is part of the energy management strategy of photosynthetic organisms that allows them to cope with the fluctuating conditions encountered in nature. Finally, unmasking the repertoire and control of such energetic reactions offers new directions for rational redesign and optimization of photosynthesis to satisfy global demands for food and other resources.

photosynthesis | starch metabolism | alternative electron outlets | FLV | PTOX

Photosynthetic organisms evolved the capacity to transform solar energy to chemical bond energy stored in C backbones that fuel most biosynthetic processes. The photosynthetic "light reactions" drive the oxidation of water by photosystem II (PSII) and both linear photosynthetic electron flow and cyclic photosynthetic electron flow (CEF) that ultimately generate ATP, NADPH, and other reduced electron carriers, including ferredoxins and thioredoxins (Fig. 1); these compounds support the energetic demands of most cellular processes. While light-driven electron transport can be described as an energy generator, a second set of photosynthetic reactions that comprise the Calvin–Benson–Bassham cycle (CBBC) utilizes the ATP and NADPH for the fixation of CO_2 into simple phosphorylated organic C compounds such as glyceraldehyde 3-phosphate (G3P) and fructose 6-phosphate (F6P). Some CBBC enzymes are indirectly activated by light through a redox switch controlled by thioredoxin. Hence, before activation, photosynthetic electron transport (PET) and C metabolism are not optimally coupled. Full activation of CBBC enzymes during a dark-to-light transition, which can increase their activities by up to 40-fold, can take 2 to 3 min (1–3).

The anabolic use of photosynthetically derived electrons and ATP is governed by an extensive network of integrated reactions that ultimately couples the products of the light reactions with downstream C metabolism. An efficient coupling promotes cell growth and division as well as the storage of energy-rich, organic polymers. However, environmental fluctuations in light, nutrient availability, and other abiotic factors may create an imbalance between the products of the photosynthetic light reactions and their utilization by the CBBC. Under such circumstances, the overflow of energetic electrons generated by photosystem I (PSI) and PSII can be photochemically quenched via a number of O_2-reducing pathways that occur within chloroplasts; some of these reactions have been designated H_2O-to-H_2O (water-to-water) cycles (4, 5). The H_2O-to-H_2O "electron outlets" include Mehler-type reactions (6, 7), in which O_2 is directly reduced by electrons to form H_2O on the acceptor side of PSI, a process that can also result in the generation of reactive oxygen species (ROS). Electrons can also be dissipated through a PSI-dependent enzymatic reaction catalyzed by specific heterodimeric flavodiiron proteins (FLVs, NADPH:flavin oxidoreductase) that directly reduce O_2 to H_2O without the release of ROS (8–10) (Fig. 1). Mutant organisms unable to synthesize FLVs exhibit compromised growth when exposed to fluctuating light as a result of oxidative damage caused by ROS accumulation and a decline in PSI activity (8–11). Moreover, FLVs can prime PSII electron flow, O_2 evolution, and lumen acidification under conditions in which the CBBC enzymes are not fully activated (8, 12). Chlororespiration represents an additional outlet in which electrons of quinols in the plastoquinone (PQ) pool

Significance

Most forms of life on Earth cannot exist without photosynthesis. Our food and atmosphere depend on it. To obtain high photosynthetic yields, light energy must be efficiently coupled to the fixation of CO_2 into organic molecules. Suboptimal environmental conditions can severely impact the conversion of light energy to biomass and lead to reactive oxygen production, which in turn can cause cellular damage and loss of productivity. Hence, plants, algae, and photosynthetic bacteria have evolved a network of alternative outlets to sustain the flow of photosynthetically derived electrons. Our work is focused on the nature and integration of these outlets, which will inform a rational engineering of crop plants and algae to optimize photosynthesis and meet the increased global demand for food.
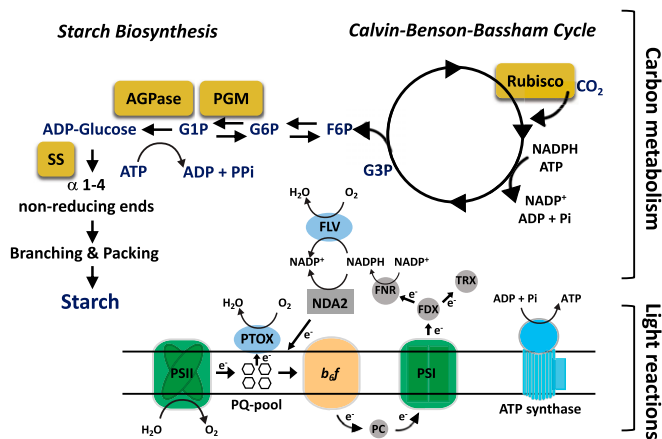
Fig. 1. Integration of photosynthetic light reactions and C metabolism. The light reactions include the reaction center/electron transport components PSI and PSII (green), cytochrome b_6f (b_6f) (orange), and ATP synthase (blue), with CBBC (cycle, *Upper Right*) and starch biosynthesis (pathway, *Upper Left*) using the products of these reactions. Metabolites: G3P, glyceraldehyde 3-phosphate; F6P, fructose 6-phosphate; G6P, glucose 6-phosphate; G1P, glucose 1-phosphate. C metabolism-related enzymes are highlighted in gold filled rectangles (Rubisco, ribulose bisphosphate carboxylase oxygenase; PGM, phosphoglucomutase; SS, starch synthase). Other enzymes/electron transfer components are PC, plastocyanin (gray-filled circle, involved in transferring electrons from cytochrome b_6f to PSI); PTOX and FLV (blue-filled ovals; involved in reducing O_2); NDA2, NADPH oxidoreductase (gray-filled rectangle; moves electrons into the PQ pool); FDX, ferredoxin; TRX, thioredoxin; FNR, flavin:NADPH reductase (gray-filled circles; moves electrons out of the electron transport chain).

can be used to reduce O_2 to H_2O through the plastid terminal oxidase (PTOX, plastoquinol:oxygen oxidoreductase; Fig. 1) (13–15). This reaction can be coupled with PSII-driven electron transfer from H_2O, or by NADPH, which can reduce PQ through the NAD(P)H-PQ reductase (16–19). It was previously demonstrated that PTOX controls the redox state of the PQ pool in the dark and may act as a safety valve during periods of environmental stress (15, 20). Another process that can photochemically quench energized photosynthetic electrons is photorespiration. This reaction, which involves the oxygenation activity of Rubisco, is an O_2-consuming pathway that can be significant when cellular CO_2 levels are low and light levels are high (21). Photosynthetic electrons can also be used by hydrogenases to reduce protons and synthesize molecular hydrogen (22, 23) or can exit plastids in the form of organic compounds such as malate or triose-phosphate through the activity of the malate-oxaloacetate and triose phosphate redox shuttles and be consumed by mitochondrial respiratory pathways (24–30).

Starch biosynthesis is another electron outlet; it involves a set of anabolic reactions that couple the use of NADPH and ATP generated by the photosynthetic light reactions with building and storing C polymers. Starch polymers (or granules), synthesized in the plastids of vascular plants and green algae, are essential for the viability of photosynthetic organisms in their natural habitat. Aside from being a repository for fixed C, starch polymers form structural components and represent a sustainable outlet (i.e., the energy within the polymer can be reused) for reductant and ATP. In plant leaves, starch transiently accumulates during the day and is used at night to fuel respiration, while in non-photosynthetic organs it provides the energy for growth and development (31–34). In the green unicellular alga *Chlamydomonas reinhardtii* (hereafter Chlamydomonas), starch synthesis has been noted over the past two decades to be part of the cell's "energetic management" strategy that becomes critical when light energy is not efficiently converted into growth (biomass), often in response to suboptimal environmental conditions such

as low nutrient availability (refs. 35 and 36 and reviewed in ref. 37). The pathway for starch synthesis requires several enzymes, as shown in Fig. 1 (reviewed in ref. 38) and is fueled by ATP derived primarily from photosynthesis and C backbones synthesized by the CBBC. The rate-limiting step in starch synthesis involves the enzyme ADP glucose pyrophosphorylase (AGPase, encoded by the *STA6* locus) which uses ATP to convert glucose-1-phosphate (G1P) to ADP-glucose while releasing pyrophosphate (PPi) (Fig. 1). In the last few decades, various Chlamydomonas "starchless" mutants have been isolated and characterized (38). One such mutant, disrupted for the gene encoding AGPase (designated *sta6*), accumulates no detectable starch (38, 39). The *sta6* mutant also exhibited a marked reduction in photosynthetic capacity, although the mechanism underlying this phenomenon remains speculative (40, 41)

We have begun to appreciate the critical nature of the light-driven reduction of O_2 for cell survival. However, we still know little about how these electron-consuming pathways are coordinated with PET, CBBC activity, and the activity of other C assimilatory/storage pathways like starch metabolism. In this work, we explore the dynamics of alternative electron outlets during dark-to-light transitions, a situation in which PET is not optimally integrated with downstream C metabolism (the CBBC requires minutes to become activated upon exposure to light) (2). We demonstrate the importance of starch synthesis as a sustainable outlet for electrons generated by the light reactions. In the absence of this outlet, PET is impaired and PTOX activity increases, facilitating an H_2O-to-H_2O cycle that represents a nonsustainable outlet for electrons but is essential to balance the redox state of the PQ pool. We also demonstrate that the reduction of O_2, which immediately engages in cells as they transition from the dark to light and is catalyzed by the FLVs, enables electron transport when the CBBC is not fully activated. Finally, we determine the apparent maximum rate of FLV activity as well as the overall amount of O_2 being consumed by FLV at different light intensities when PET and C metabolism are not optimally integrated.

Results

Starch synthesis, a sink for reductant/fixed C and ATP, can potentially impact which of the various cellular pathways are used to consume photosynthetically derived electrons. In the absence of starch synthesis, the excess excitation that cannot be coupled to downstream C metabolism could potentially be non-photochemically quenched and/or the excited electrons may be photochemically quenched through activation of alternative pathways that deliver photosynthetically derived electrons to O_2 to generate H_2O; these pathways result in O_2 uptake. Furthermore, at the onset of a dark-to-light transition, the reactions involved in fixing CO_2 (CBBC) are not fully active and therefore are not optimally integrated with PET (2). To explore the extent of photochemical processes associated with quenching of excess excitation and how these processes are integrated with photosynthetic C metabolism, we monitored the dynamics of O_2 evolution and uptake during dark-to-light transitions in the *sta6* starchless mutant (39). As a control for this analysis, we used the genetically complemented (*sta6::STA6*) C6 strain (42). These strains were previously used for evaluating *sta6* function (35, 43–45).

Electrons Are Redirected Toward FLVs at the Onset of Light. Membrane inlet mass spectrometry (MIMS) was used to quantify O_2 production ($^{16}O_2$ evolution) and uptake (depletion of injected $^{18}O_2$ from the medium) upon exposure of *sta6* and C6 cells to increasing light intensities (50, 150, 300, and 1,000 μmol photons·m^{-2}·s^{-1}) during photoautotrophic growth in the presence of elevated CO_2 (Fig. 2). The trends for O_2 production and uptake changed to some extent over the time of the light treatment (at any

PLANT BIOLOGY

intensity used), and we therefore divided the light period (6 min in total, represented by white bars above graph in Fig. 2) into an early phase (first 3 min) and late phase (last 3 min).

When C6 cells were exposed to light after a 5-min dark pre-incubation, the rate of gross $^{16}O_2$ production rapidly increased to a maximal rate, or Pmax, and remained steady for the remainder of the light treatment (green curve, Fig. 2A). Pmax was positively correlated with an increase in light intensity and attained a maximum value of ~190 μmol O_2·mg^{-1} Chl·h^{-1} at 1,000 μmol photons·m^{-2}·s^{-1} in C6 cells (Figs. 2A and 3A). We also measured O_2 uptake by C6 cells, which exhibited a pronounced peak (Umax; maximum O_2 uptake rate) at the onset of the light (red curve Fig. 2A). The Umax, like the Pmax, was positively correlated with light intensity, attaining a rate of ~80 μmol O_2·mg^{-1} Chl·h^{-1} at 1,000 μmol photons·m^{-2}·s^{-1} during the early phase of the light period (Figs. 2A and 3A). The ratio of Umax to Pmax (Umax/Pmax), which reflects the fraction of reductant generated by the photosynthetic light reactions that is not coupled to CO_2 fixation/metabolism or nutrient assimilation (e.g., reduction of nitrite or sulfate), did not markedly vary at the different light intensities tested during the early phase of the light exposure (~0.4). It did, however, decline during the later stages of light exposure and appeared to stabilize at ~0.25 (Fig. 3A). Consequently, for C6, the rise in net O_2 production with increasing light intensity (blue curve, Fig. 2A) lagged relative to the initial rise in gross O_2 production (green curve, Fig. 2A). At all light intensities, immediately following the Umax peak the net production of O_2 rose to its maximal value, or Pmax$_{net}$ (Pmax$_{net}$ values were correlated with light intensity as well; Fig. 3A). These data agree with previous studies showing that a marked increase in O_2 uptake occurs immediately after cells are exposed to high light (HL) or during a dark-to-light transition (8, 10). Such a rise in O_2 uptake was demonstrated to reflect the activity of the FLV proteins, which use electrons on the acceptor side of PSI to reduce O_2, and as a consequence drive water oxidation and O_2 evolution by PSII and protect the photosynthetic apparatus from oxidative damage before full activation of the CBBC (8–11, 46).

Eliminating Starch Synthesis Caused Elevated O_2 Photoreduction.

Surprisingly, O_2 production and uptake by sta6 cells showed trends that were notably different from those of C6 (Fig. 2B). The mutant cells exhibited a burst of gross O_2 production (green curve, Fig. 2B) soon after they were transferred from darkness to light, followed by a gradual decline to a steady-state level of O_2 evolution. Similar to the results for C6 cells, Pmax was positively correlated with light intensity, although the level of gross O_2 evolution was almost twofold lower than the level observed for C6 (Figs. 2 and 3B). Simultaneous with the burst in O_2 production, the rate of O_2 uptake began to increase (at 150 μmol photons·m^{-2}·s^{-1} and above), reaching Umax soon after the burst of gross O_2 production (red curve, Fig. 2B). Although the Umax for sta6 and C6 were similar during the early phase of the light period (compare Fig. 3 A and B), the uptake of O_2 slowly declined in sta6 over a longer period than the decay of O_2 uptake in C6 cells (compare red curves in Fig. 2). Furthermore, the Umax/Pmax value for sta6 cells was ~0.8 during the early phase of the light period, resulting in a low rate of net O_2 production (Fig. 3B). These results suggest that a smaller proportion of reductant generated by PSII in sta6 was coupled to CO_2 fixation (or non-oxygen-related reduction reactions) relative to C6. The Umax/Pmax for sta6 decreased during the late phase of the light period (0.5 to 0.6; Fig. 3B), suggesting reduced activity of pathways that use O_2 as a terminal acceptor of electrons relative to those in which the terminal acceptor is not O_2.

To extend these findings, we compared the MIMS data to PET through PSII based on chlorophyll fluorescence (SI Appendix, Fig. S1A). The maximal PSII quantum efficiency (Fv/Fm) was similar for C6 and sta6 (0.65 ± 0.00 and 0.66 ± 0.02, respectively; SI Appendix, Fig. S1A), suggesting that sta6 suffers no more damage to PSII than C6 under the conditions used to culture the strains. Furthermore, only a minor difference was observed in the quantum yield of PSII (ΦPSII) for C6 and sta6 (slightly lower for sta6) when the cells were exposed to up to ~165 μmol photons·m^{-2}·s^{-1}. When the light intensity was raised above 165 μmol photons·m^{-2}·s^{-1}, the difference in ΦPSII between sta6 and C6 became slightly greater (15 to 25% difference), although it
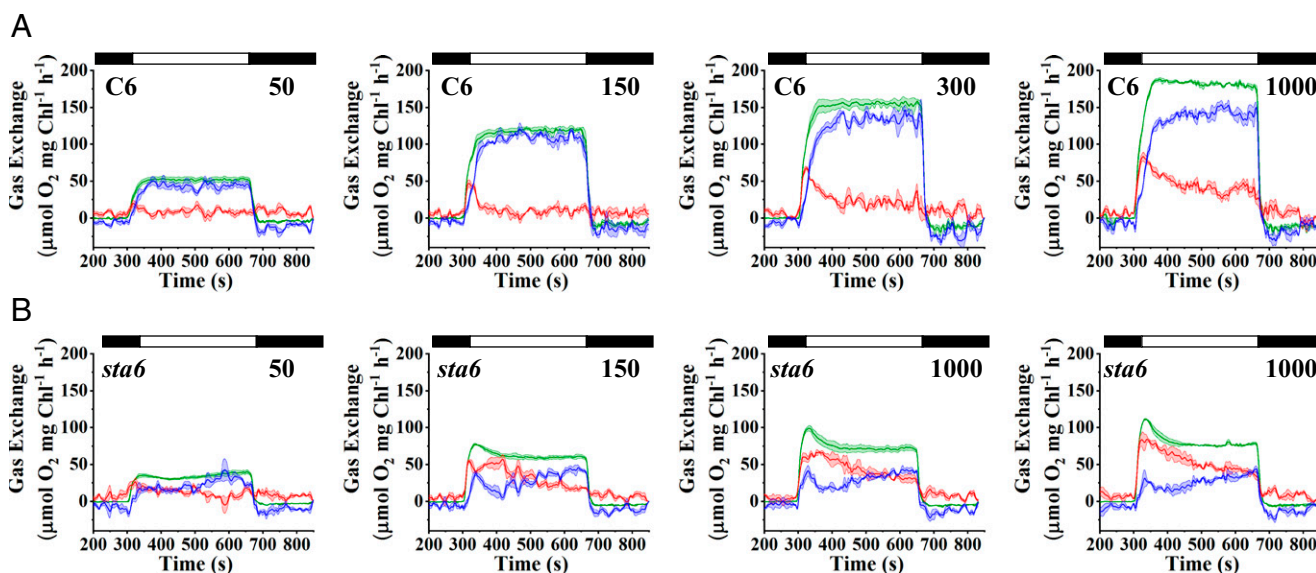

Fig. 2. Light-induced O_2 evolution and uptake. C6 (A) and sta6 (B) were cultured photoautotrophically, bubbled with 2% CO_2 in air, and maintained in continuous light of 100 μmol photons·m^{-2}·s^{-1}. Gross O_2 production ($^{16}O_2$ evolution, green curve) and light-induced uptake of O_2 ($^{18}O_2$ uptake, red curve) were monitored for 6 min using MIMS at four different light intensities (50, 150, 300, and 1,000 μmol photons·m^{-2}·s^{-1}, as indicated in the upper right of each graph). Before turning on the light, the cells were maintained for 5 min in the dark (black bars on the top, left of each graph), and for an additional 3 min in the dark following the illumination (black bar, on the top, right of each graph). Gross O_2 uptake and both gross and net (blue curve) O_2 production were calculated according to the formula given in Materials and Methods. Each trace represents an average of at least three biological replicates ± SE.
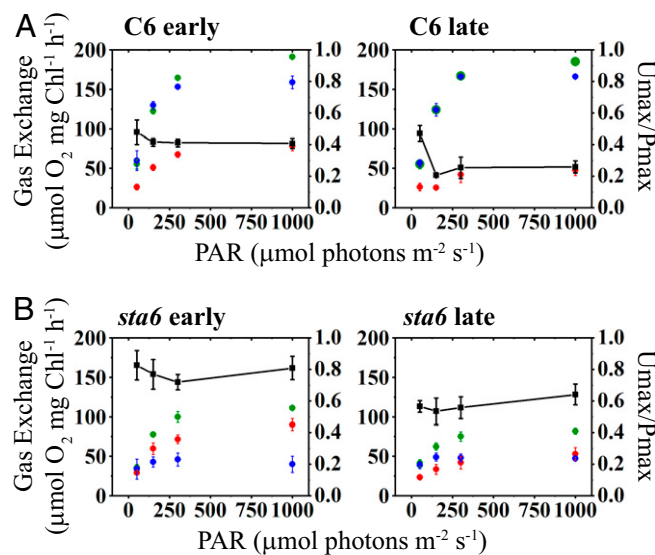
Fig. 3. Maximal rates of light-induced O_2 production and uptake. Maximal values for gross and net O_2 production (green and blue, respectively) and gross O_2 uptake (red) for C6 (A) and sta6 (B) are plotted as a function of light intensity. The left-hand y axis gives gross and net O_2 evolution and gross O_2 uptake. The right-hand y axis gives the ratio of maximal gross O_2 uptake relative to maximal gross O_2 production; this value is plotted as a function of light intensity (black line with black squares). For both A and B, the left panel presents the data for the first 3 min of the light phase and the right panel presents the data for the final 3 min of the light phase (i.e., early and late periods during illumination, respectively; see main text for details). Net O_2 evolution was calculated as gross O_2 production – gross O_2 uptake. Each point is an average of at least three biological replicates ± SD.

does not explain the pronounced difference in gross O_2 production between the strains based on MIMS measurements. This difference could be the consequence of cyclic electron flow around PSII (47) in sta6 (see *Discussion*).

Taken together, these O_2 exchange analyses for C6 and sta6 suggest that a defect in starch biosynthesis and the consequent loss of an outlet for electrons/fixed C and ATP resulted in a greater proportion of the light-generated electrons being directed toward outlets that involve O_2 reduction. Furthermore, a peak in light-dependent O_2 uptake in C6 occurred soon after the cells were exposed to light and before a rise in net light-dependent O_2 production. This O_2 uptake likely reflects FLV protein activity, which has been shown to engage immediately after the onset of light (8, 10, 11, 46). Importantly, sta6 cells exhibited a unique $^{18}O_2$ uptake pattern reflected by a broader peak (lasting a few minutes) than in C6. This suggests that the activity of the FLV proteins is more sustained in the mutant and/or that more than one component may contribute to photoreduction of O_2.

Interactions Between Starch Synthesis and O_2 Photoreduction. To further elucidate the nature of light-dependent O_2 uptake and potential participation of alternative electron outlets during the transition from dark to light, we analyzed the kinetics of O_2 production and uptake for C6 and sta6 cells in more detail (Fig. 4; cells were exposed to 300 μmol photons·m^{-2}·s^{-1}). Although the rate of gross O_2 production was lower in sta6 than in C6 (Figs. 2 and 3), the kinetics of the initial rise of gross O_2 production over the first 20 s of the light period was similar between the strains (linear fitting of the initial rise of $^{16}O_2$ production; slopes are 4.5 and 4.1 for C6 and sta6, respectively; Fig. 4A, dashed-dotted curves). Furthermore, during this period, the two strains exhibited similar kinetics for the rise in $^{18}O_2$ uptake (the rise in O_2 uptake was fitted to a first-order exponential decay type curve and

values τ = 2.4 s^{-1} and 2.0 s^{-1} for C6 and sta6, respectively; t test, P = 0.23; Fig. 4A), suggesting that a similar mechanism may be involved in eliciting the initial light-driven production and uptake of O_2 for the two strains. However, while $^{18}O_2$ uptake for C6 cells decayed to a basal level soon after Umax was attained, the rate of O_2 uptake in sta6 cells remained constant for at least 100 s followed by a slow decay (Fig. 4A, Inset). Overall, sta6 cells showed a threefold slower decay rate than C6 cells (slopes are −0.15 and −0.46 for C6 and sta6, respectively; $^{18}O_2$ uptake curves for a longer time period are shown in Fig. 4A, Inset). These observations demonstrate that the starchless mutant directed a greater proportion of electrons to photochemistry associated with the uptake of O_2 over the entire light period relative to the complemented strain.
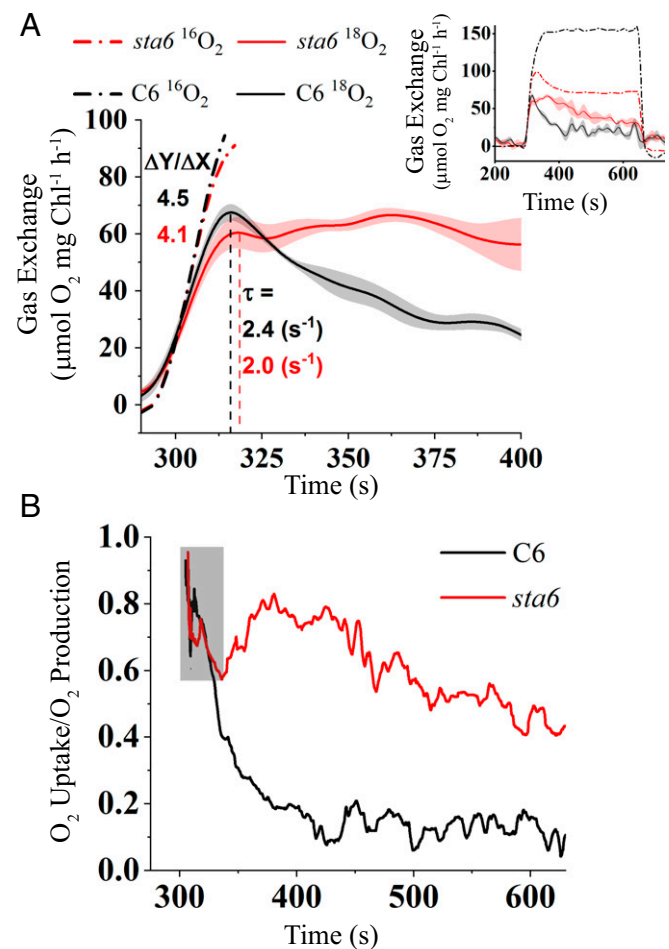

Fig. 4. Kinetics of light-induced O_2 production and uptake. (A) MIMS traces of $^{16}O_2$ evolution (gross production, dotted-dashed lines) and $^{18}O_2$ uptake (gross uptake, solid lines) during dark-to-light transition (300 μmol photons·m^{-2}·s^{-1}) for C6 (black) and sta6 (red). Gross O_2 production ($^{16}O_2$) data during the first 20 s of the light period was linearly fitted and the initial rates (ΔY/ΔX) calculated (black and red dash-dotted lines). The $^{18}O_2$ uptake curves were fitted to first-order exponential decay curves to determine the rate (τ) at which a peak of $^{18}O_2$ uptake for C6 and sta6 was attained (dashed black and red line for C6 and sta6, respectively). (Inset) Presentation of the MIMS traces for gross O_2 evolution and uptake during the entire light period (SE is only shown for gross O_2 uptake for both sta6 and C6). (B) The ratio of gross $^{18}O_2$ uptake to $^{16}O_2$ production during the light period (300 μmol photons·m^{-2}·s^{-1}). Same conditions as in A. Gray box highlights the region in which the decline in the ratio for C6 and sta6 cells is similar. Each data line represents an average of three biological replicates.

We also observed this phenomenon when we compared the ratio of gross uptake and production of O_2 in C6 and *sta6* cells (Fig. 4*B*). Immediately after the cells were exposed to light, the ratio of O_2 uptake to production was over 0.9 for both strains. After 20 to 30 s in the light, this ratio similarly declined to ~0.6 (as a result of a similar increase in gross O_2 production; highlighted in gray box) in both C6 and *sta6* cells. However, while this ratio continued to fall to ~0.1 for C6 cells, the proportion of O_2 uptake to production for *sta6* increased to ~0.8 after 100 s and remained much higher than that of C6 cells along the entire 6-min light period (Fig. 4*B*). Comparable trends were found when the cells were exposed to lower or higher light intensities (50, 150, and 1,000 µmol photons·m^{-2}·s^{-1}; *SI Appendix*, Fig. S2).

In sum, immediately following exposure of the cells to light, the CBBC is not fully activated and the high-energy electrons generated by PET cannot immediately be used for CO_2 fixation. Under such circumstances, the cells, regardless of whether they have the capacity to store C as starch, share a common electron outlet, the FLV proteins, which sustains PSII-dependent O_2 production with the concomitant reduction of O_2 to H_2O. Moreover, the altered kinetics of O_2 uptake and decay in *sta6* (slower decay of $^{18}O_2$ uptake and a much higher $^{18}O_2$ uptake/$^{16}O_2$ evolution ratio during much of the light period) suggest that as compensation for the loss of starch synthesis, *sta6* cells exhibit more sustained reduction of O_2 than C6, supporting the possibility that there is more than one component contributing to O_2 uptake during the light period. These results also raise the possibility that activation of the CBBC (or downstream reactions) is slower for the mutant than for the complemented cells, resulting in an increased contribution of FLV to the reduction of O_2 in the mutant (the CBBC and FLV compete for the same pool of electrons). Alternatively, slower activation of CBBC and consequently a decrease in the pool of downstream electron acceptors resulting from the loss of starch synthesis in *sta6* feeds back on electron transport, causing hyperreduction of the PQ pool, which in turn may activate PTOX and result in increased O_2 consumption. Additionally, we cannot rule out the possibility that mitochondrial respiration becomes a more dominant contributor to total $^{18}O_2$ uptake in *sta6*. However, this possibility seems less likely since the O_2 uptake rate measured in the dark (immediately following the light-to-dark transition) is slower in *sta6* than in C6 (*SI Appendix*, Fig. S1*B*). Finally, photorespiratory O_2 uptake would likely be a minor component to gas exchange since all of our experiments were performed at a high concentration of CO_2, which inhibits photorespiration (48).

Contribution of PTOX to O_2 Uptake in *sta6*. To further probe potential contributions of the FLVs and assess the role of PTOX in routing electrons during a transition from darkness to light, we supplemented cultures with 2 mM propyl gallate (PG), a reagent that inhibits alternative oxidases such as PTOX but does not inhibit FLV activity. This inhibitor was added to cultures at the beginning of the dark period (5 min before light exposure) and its impacts on O_2 production and uptake were monitored during the light (300 µmol photons·m^{-2}·s^{-1}) period. PG did not affect the overall trends of O_2 production and uptake in C6 cells; however, the Pmax (both net and gross) was ~60% of the value measured in the absence of PG (Fig. 5*A* and *SI Appendix*, Table S1). In contrast, in PG-treated *sta6* cells the initial burst of gross $^{16}O_2$ production was completely suppressed and Pmax was 46% of that of untreated *sta6* cells (Fig. 5*B* and *SI Appendix*, Table S1); a similar rate of $^{18}O_2$ uptake and $^{16}O_2$ production resulted in zero net O_2 production for the first 2 min following exposure of the cells to light (Fig. 5*B*). As the length of exposure to the light increased, $^{18}O_2$ uptake slightly declined while both net and gross $^{16}O_2$ evolution gradually rose (Fig. 5*B*).

Umax of both untreated and PG-treated C6 cells was attained at approximately the same time following exposure to light, but the Umax value of PG-treated C6 cells was ~68% of that of untreated cells (Fig. 5*C* and *SI Appendix*, Table S1; Umax for untreated and treated cells are indicated with a solid and dashed red line, respectively, extended from the *x* axis) and the rate at which Umax was attained was slower by more than twofold (initial slopes of 1.9 and 4.4 for PG-treated and untreated C6, respectively; Fig. 5*C*). For *sta6*, untreated cells attained Umax 15 s faster than for PG-treated cells. The Umax value of PG-treated cells was ~60% of that of untreated cells (Fig. 5*D* and *SI Appendix*, Table S1; Umax for untreated and treated cells are indicated with a solid and dashed red line, respectively, extended from the *x* axis) and the rate at which the Umax was attained was slower by ~3.5-fold (Fig. 5*D*; initial slopes of 0.9 and 3.2 for PG-treated and untreated *sta6* cells, respectively). However, the overall trend of $^{18}O_2$ uptake in *sta6* cells following the initial rise was not markedly impacted; the rate of O_2 uptake remained constant for an initial period of ~100 s in the light and then gradually slowed, but high values of Umax/Pmax were maintained over the entire light period (~125%; Fig. 5 *B* and *D* and *SI Appendix*, Table S1).

Since PTOX modulates the redox state of the PQ pool (15, 20, 49), its inhibition by PG before the light period could limit oxidation of the quinol pool (in the dark), which would lead to a decline in the rates of both light-driven O_2 production and uptake, a lower Pmax, and a slower rise in the uptake of O_2, as shown in Fig. 5 *C* and *D*. To explore this possibility, we measured the redox state of the PQ pool, as 1-qL (50), after exposing PG-treated and untreated cells to 300 µmol photons·m^{-2}·s^{-1} for 1 min. For untreated cells, the PQ pool was 30% more reduced in *sta6* than in C6 (1-qL value was 0.63 ± 0.01 and 0.49 ± 0.06, respectively; Fig. 5*E*), reflecting a feedback of compromised starch synthesis on electron transport. Upon PG treatment, the reduction state of the PQ pool of both C6 and *sta6* increased by ~25%, but it was more reduced in *sta6* than in C6 cells (0.83 ± 0.00 and 0.61 ± 0.06, respectively; Fig. 5*E*). These findings suggest that slower rates of O_2 production could be a consequence of elevated reduction of the PQ pool resulting from PTOX inhibition; however, the impact of this inhibition is much more pronounced in *sta6* cells. Furthermore, when we measured the redox state of the PQ pool as a function of increased light intensity, we found that C6 cells treated with PG maintained a redox state close to that of untreated cells over the entire light range (Fig. 5*F*, compare magenta and pink triangles). Hence, PTOX appears to have a minor impact on total light-driven uptake of O_2 when starch metabolism is not impaired (i.e., in C6 cells) but is important when the cells are maintained in the dark. In contrast, the PQ pool of PG-treated *sta6* cells was more reduced than the nontreated cells at all light intensities (Fig. 5*F*, compare magenta and pink circles), but especially at low/moderate intensities, suggesting that the PG-treated *sta6* cells are compromised in their ability to oxidize the PQ pool, likely a consequence of an additive effect of PTOX inhibition and an inability to synthesize starch in the light. Together, these experiments suggest that PTOX is essential for balancing the redox state of the PQ pool when the cells are maintained in the dark. Furthermore, eliminating PTOX activity slows the rate of O_2 production upon shifting the cells to the light regardless of whether the cells can synthesize starch. Moreover, the finding that PG-treated *sta6* cannot maintain the redox state of the PQ pool (unlike PG-treated C6; Fig. 5*F*) suggests that the loss of starch synthesis eliminates an important electron outlet that may elicit feedback inhibition of CBBC and/or electron transport, which leads to an increase in excitation pressure on the PQ pool.

Synthesis of Starch as an Alternative Outlet. To further explore the role of starch synthesis as an alternative outlet for C, we analyzed the levels of phosphorylated sugar intermediates focusing on the conversion of F6P to metabolites related to CBBC activity
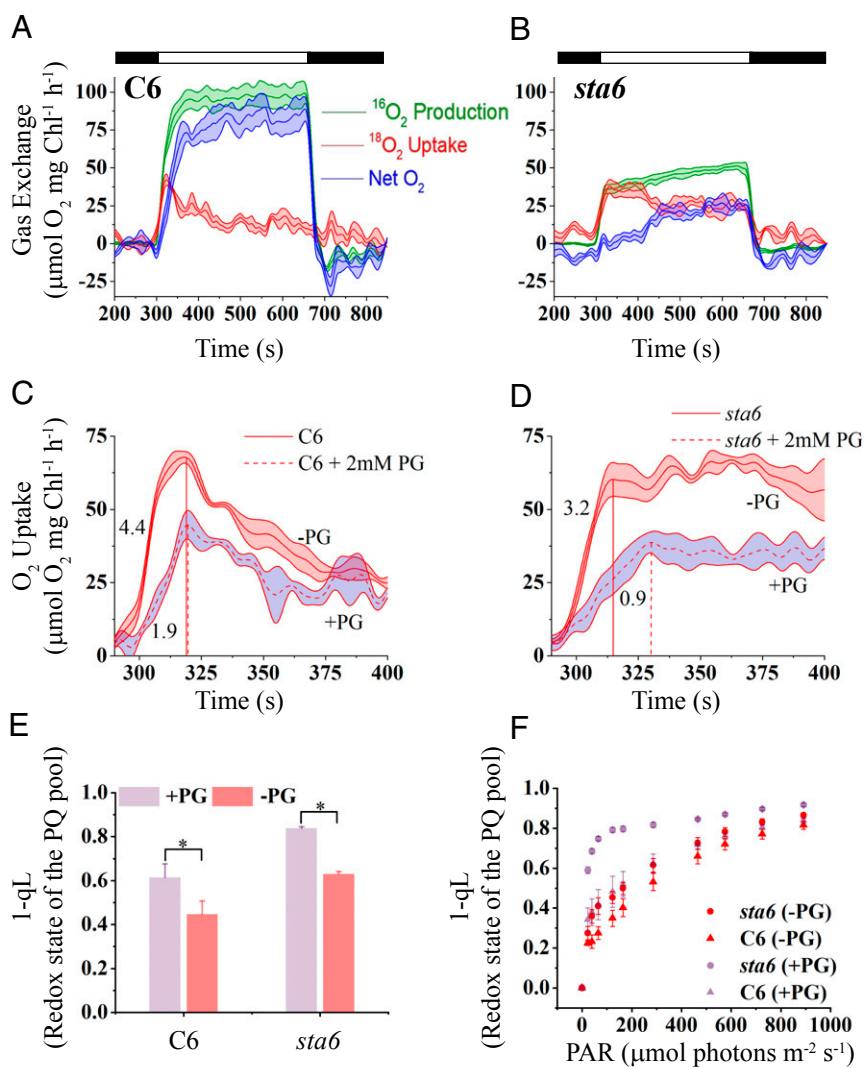
Fig. 5. Effect of a PTOX on O_2 production and light-induced O_2 uptake. C6 (*A*) and *sta6* (*B*) were exposed to 300 µmol photons·m^{-2}·s^{-1} (white bars) in the presence of 2 mM PG and gas exchange was analyzed using MIMS, as in Fig. 3 (see Fig. 3 legend). Comparisons of the first 2 min of $^{18}O_2$ uptake for C6 (*C*) and *sta6* (*D*) in the presence (dashed line with purple shading) and absence (solid line with red shading) of PG. The time (seconds) to achieve Umax for C6 and *sta6* is highlighted by dotted red lines that extend from the *x* axis to the Umax peak. Each trace represents an average of at least three biological replicates with the shaded area associated with each trace representing the SE. (*E*) 1-qL values of PG-treated/untreated cells. The cells were PG-treated during the 5-min preincubation in the dark and then exposed to 300 µmol photons·m^{-2}·s^{-1} for 1 min. $n = 3 \pm$ SD * *t* test, $P = 0.01$. (*F*) The 1-qL values of PG-treated/untreated cells exposed to increasing light intensities. Cells were exposed to each intensity for 30 s before raising the intensity. $n = 3 \pm$ SD.

(xylulose-5-phosphate, X5P, and ribulose-5-phosphate, R5P, metabolites in the pathway leading to the regeneration of ribulose-1,5-bisphosphate, RuBP) and metabolites associated with gluconeogenesis and starch synthesis (glucose 6-phosphate, G6P, and glucose-1-phosphate, G1P) at different time points following the transition from darkness to light (300 µmol photons·m^{-2}·s^{-1}; Fig. 6 and *SI Appendix*, Fig. S3 and Table S2). In C6 cells, within the first 60 s in the light (the time in which O_2 uptake started to decline after reaching its peak; Fig. 4*A*) the levels of F6P increased by almost fourfold relative to that of dark-acclimated cells. Furthermore, the levels of G6P and G1P increased by about 5- and 2.5-fold, respectively. In contrast, the levels of X5P and R5P did not vary much from the values measured in the dark. A similar trend was detected when we repeated the experiment with *sta6* cells (Fig. 6 and *SI Appendix*, Fig. S3 and Table S2); the levels of G6P and G1P increased by more than three and twofold relative to the dark-acclimated state while the levels of X5P and R5P did not change. However, the concentration of G6P and G1P measured for *sta6* cells was much lower than that of the C6 cells (G6P: 28.60 ± 2.47 and 7.7 ± 0.4 ng/10^6 cells; G1P: 169.54 ± 8.99 and 59.4 ± 6.7 ng/10^6 cells for C6 and *sta6*, respectively; Fig. 6 and *SI Appendix*, Table S2), possibly indicating that starch synthesis has a regulatory role on CBBC enzyme activity. Finally, since *sta6* cannot synthesize starch, the levels of G6P and G1P keep increasing after 2 min in the light while they decline somewhat in C6 cells

(*SI Appendix*, Fig. S3). Taken together, these results indicate that there is an increase in the flow of C toward starch biosynthesis soon after the dark-acclimated cells are exposed to light.

Overall Contribution of FLV to Photoreduction of O_2. In prior work (8–11) it was shown that the FLV proteins are a prominent outlet for electrons when the light is first turned on and PET is not optimally integrated with downstream C metabolism. Moreover, in C6 cells, which have normal starch biosynthesis, we observed a burst of O_2 uptake and a change in the PQ redox state during the dark-to-light transition that was little impacted when PTOX was inhibited (Fig. 5*F*). Therefore, FLV is likely the dominant activity responsible for the O_2 uptake in C6 immediately following the dark-to-light transition. Hence, we sought to quantitatively evaluate the role of the FLV proteins in the reduction of O_2 during the dark-to-light transition. To quantify the contribution of FLV activity to O_2 uptake, we calculated the basal rate of light-driven O_2 uptake using a linear fit of the $^{18}O_2$ uptake data at steady state at various light intensities (late phase of light period), shown in Fig. 2*A* (*SI Appendix*, Fig. S4*A*). This uptake rate was correlated with uptake resulting from dark respiration based on O_2 electrode measurements (Pearson correlation, $r = 0.923$, $P < 0.05$; *SI Appendix*, Fig. S4*B*). Fig. 7*A* presents the overall O_2 uptake for C6 cells exposed to four different light intensities (solid lines are 50, 150, 300, and 1,000 µmol photons·m^{-2}·s^{-1}). Also shown are the calculated basal rates of O_2 uptake (which is probably
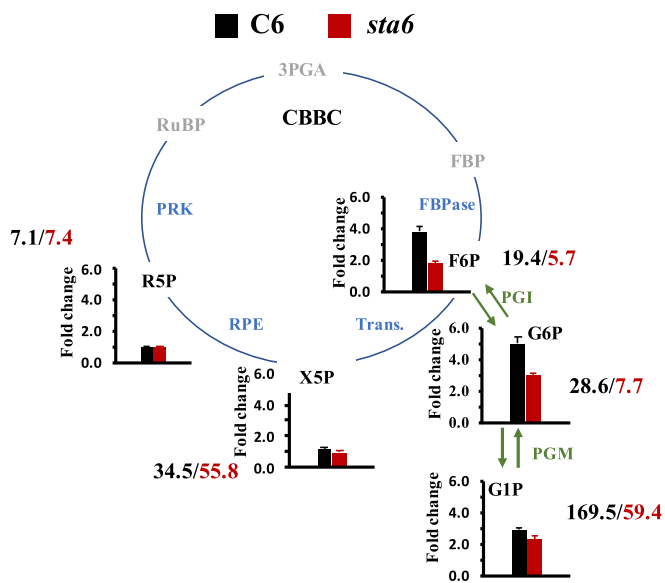
Fig. 6. Conversion of F6P of CBBC to metabolites associated with starch synthesis: Metabolite profiling following exposure of C6 and *sta6* cells (black and red bars of bar graphs, respectively) to light for 60 s. The pathway for starch biosynthesis is highlighted by green arrows and the CBBC is given as a cycle (CBBC enzymes in blue). Quantified metabolites are shown in black. The numbers next to each metabolite represent the concentration of the metabolite (nanograms per 10^7 cells) following a 60-s exposure to light. Each bar graph represents four to six biological replicates ± SE. Metabolites: F6P; G6P; G1P; X5P; R5P; RuBP; 3PGA, 3-phosphglyceraldehyde; FBP, fructose 1,6-bisphosphate. Enzymes: PGI, phosphoglucoisomerase; PGM, phosphogluco-mutase; Trans., transaldolase; RPE, ribulose phosphate 3-epimerase.

dominated by mitochondrial respiration) at the different light intensities (horizontal dashed lines with the same colors as curves for $^{18}O_2$ uptake). By integrating the area under the O_2 uptake curve using a baseline value established for the basal O_2 uptake at each of the four light intensities (e.g., see *SI Appendix*, Fig. S4C), we calculated the total amount of consumed O_2 that is associated with shifting the cells from dark to light and likely a consequence of FLV activity. The amount of O_2 consumed by putative FLV activity increased with increasing light intensities. At 300 µmol photons·m^{-2}·s^{-1}, the FLV proteins consumed 0.46 ± 0.04 µmol O_2·mg Chl^{-1}, with maximum consumption at 1,000 µmol photons·m^{-2}·s^{-1} (0.682 ± 0.16 µmol O_2·mg Chl^{-1}; Fig. 7B). Interestingly, the maximal rate of O_2 uptake (V_{max}) that we attributed to FLV activity was 45.7 ± 4.2 µmol O_2·mg Chl^{-1}·h^{-1} when the cells were exposed to 300 µmol photons·m^{-2}·s^{-1}. This rate is not significantly different from the rates measured for cells exposed to 150 or 1,000 µmol photons·m^{-2}·s^{-1} (Fig. 7C). Therefore, while FLV proteins operate at V_{max} even upon exposure to moderate light intensities, the amount of O_2 consumed following the transfer of the cells to increasing intensities of light appears to be a consequence of prolonged activation of the FLV (more sustained uptake at higher light intensities).
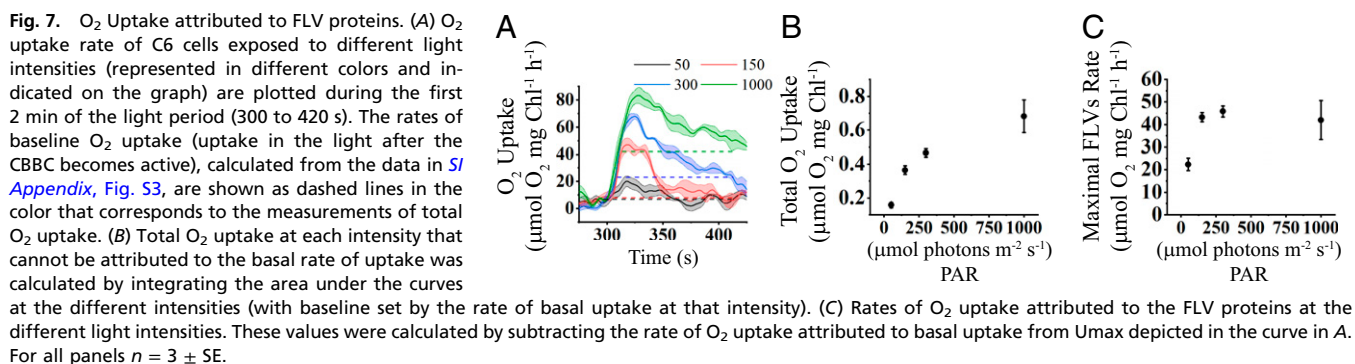
Discussion

In nature, photosynthetic organisms are frequently exposed to abiotic stresses, including marked variations in temperature and light intensities and suboptimal nutrient concentrations. Such environmental restrictions limit the growth/development of organisms and dramatically impact the use of photosynthetically generated electrons for CO_2 fixation. To cope with environmental challenges, photosynthetic organisms have developed several strategies to manage excitation energy and reroute electrons to alternative pathways. To uncover the nature of various alternative pathways for electron flow and the flexibility of the energetic

circuitry, we adopted an integrated approach to analyze the dynamics associated with photoreduction of O_2 through FLV and PTOX activities and photosynthetic C metabolism, including starch synthesis, during dark-to-light transitions, a condition under which PET and C metabolism are not in equilibrium. The *sta6* mutant (42), which is unable to synthesize starch, was used to evaluate how the flow of C toward starch impacts electron flow during the dark-to-light transition.

Elimination of starch synthesis in Chlamydomonas resulted in a pronounced decrease in light-dependent O_2 evolution (Figs. 2 and 3), suggesting interactions between PET and downstream processes that consume electrons. Real-time analyses of gross O_2 exchange using isotopically labeled O_2 to distinguish between production ($^{16}O_2$) and light-driven uptake ($^{18}O_2$) demonstrated that *sta6* cells exhibited more sustained light-induced reduction of O_2 that was as high as 80% of the gross O_2 evolution (compared with 20 to 40% for C6 cells), and consequently the mutant cells had low net O_2 evolution (Figs. 2, 3, and 4B). The lower maximal $^{16}O_2$ production and the elevated ratio of O_2 uptake to production (reflecting the fraction of reductant not used for CO_2 fixation and growth) highlights an essential role for starch synthesis as a transient outlet for storing reductant/energy generated by PET as the cells are activating downstream C metabolism. Furthermore, despite the lower rates of gross O_2 production exhibited by *sta6* relative to C6 cells, we did not observe a dramatic decrease in electron flow through PSII (measured as ΦPSII; *SI Appendix*, Fig. S1A) when the cells were exposed to light intensities as high as 300 µmol photons·m^{-2}·s^{-1}. This discrepancy may be explained by activation of cyclic electron flow around PSII (PSII-CEF). Although this type of alternative pathway has not been intensively investigated, several studies suggest that PSII-CEF is activated under conditions in which the PQ pool is highly reduced (47, 51–53). A potential role for PSII-CEF in *sta6* cells requires additional investigation.

Genes encoding FLV proteins are present in prokaryotes, green algae, mosses, liverworts, lycophytes, and gymnosperms but are not found in vascular plants (54). These proteins function as an outlet for electrons when C metabolism is not optimally coupled to the rate of photosynthetic electron flow (8–11). Our analyses revealed a rapid increase in light-driven reduction of O_2 that takes place soon after Chlamydomonas cells are transitioned from the dark to the light. The kinetics of this "burst" of O_2 uptake was similar for C6 and *sta6* (~2.4 s^{-1} at 300 µmol photons·m^{-2}·s^{-1}; Fig. 4A) and is consistent with a function of FLVs in priming PET (8) and harmlessly dissipating high-energy electrons before the activation of the CBBC and downstream C metabolism. In this context, recent work has demonstrated that slowed electron transport in *Arabidopsis* resulting from a defect in CEF [*pgr5* mutant, associated with CEF control (55)] could be reversed by transforming the mutant plants with the *FLV* genes (54). Similarly, a Chlamydomonas *pgr5* mutant accumulates FLVs when the cells are exposed to HL (12). In these two examples, FLVs provide an alternative route for an "overflow" of electrons (more electrons produced by the light reactions than can be used by downstream anabolic processes) by redirecting them toward the reduction of O_2 to generate H_2O. Importantly, our analyses allowed us to estimate the energy loss through dissipation of electrons by FLV-mediated photoreduction during the dark-to-light transition and the maximum rate of electron flow from FLV to O_2. C6 cells shifted from dark to light revealed a V_{max} for O_2 uptake by FLV of ~45 µmol O_2 mg·Chl^{-1}·h^{-1} under the conditions of our study (Fig. 7C), which is equivalent to 22.5 e$^-$·s^{-1}·PSI^{-1} (conversion between units was done according to ref. 56). A threshold for V_{max} could limit the capacity of electron dissipation under conditions of high photon flux. We therefore also measured the total O_2 uptake by the FLV proteins at different light intensities (Fig. 7A and *SI Appendix*, Fig. S4C). Based on our calculations, the total amount of O_2

Fig. 7. O$_2$ Uptake attributed to FLV proteins. (*A*) O$_2$ uptake rate of C6 cells exposed to different light intensities (represented in different colors and indicated on the graph) are plotted during the first 2 min of the light period (300 to 420 s). The rates of baseline O$_2$ uptake (uptake in the light after the CBBC becomes active), calculated from the data in *SI Appendix*, Fig. S3, are shown as dashed lines in the color that corresponds to the measurements of total O$_2$ uptake. (*B*) Total O$_2$ uptake at each intensity that cannot be attributed to the basal rate of uptake was calculated by integrating the area under the curves at the different intensities (with baseline set by the rate of basal uptake at that intensity). (*C*) Rates of O$_2$ uptake attributed to the FLV proteins at the different light intensities. These values were calculated by subtracting the rate of O$_2$ uptake attributed to basal uptake from Umax depicted in the curve in *A*. For all panels $n = 3 \pm$ SE.

consumption associated with the dark-to-light burst increased as a function of light intensity (ranging from 0.15 to 0.7 μmol O$_2$·mg Chl^{-1} for C6; Fig. 7*B*). This increased photochemical dissipation is reflected by a broadening of the O$_2$ uptake peak that resulted because of a slower decay in O$_2$ uptake (Fig. 7*A*). This slowed decay may be part of a compensation mechanism that diverts electrons to FLV when the redox pressure on the CBBC and perhaps downstream C utilization processes increase because these pathways are not yet fully activated.

While FLVs maintain PET during the transition from dark to light through reduction of O$_2$, C intermediates rapidly flow toward starch synthesis, as indicated by an increase in the concentration of G6P and G1P after 60 s following dark-to-light transitions (Fig. 6 and *SI Appendix*, Fig. S3 and Table S2). In contrast, there was little change in the levels of X5P and R5P over a 5-min exposure of the cells to light. The accumulation of G6P and G1P in C6 cells aligned with the decrease of the initial O$_2$ uptake burst (Fig. 4*A* and *SI Appendix*, Fig. S3) and is congruent with the time needed for redox activation of FBPase [catalayzes conversion of F1,6BP to F6P (3, 57)] and the slightly slower activation of PRK [catalyzes conversion of R5P to RuBP (3, 58)]. In *sta6* cells the concentrations of phosphorylated sugar intermediates were much lower than in the C6 complemented line (Fig. 6 and *SI Appendix*, Table S2). We therefore raise the possibility that the starch metabolic pathway has a regulatory effect on CBBC enzymes which explains the strain's low gross O$_2$ production (Figs. 2*B* and 3), not only in Chlamydomonas but also in *Arabidopsis* (41). Further analyses are required to describe the mechanism underlying this regulatory effect. Based on these findings, we propose that the starch biosynthesis pathway is activated soon after the light is switched on and drains C metabolites out of the CBBC to prevent feedback inhibition on CBBC's enzymes while they are not fully active; hence, this pathway may facilitate activation of the CBBC and sustain PET.

Other electron valves may also play a role in sustaining nondestructive electron transport during dark-to-light transitions. PTOX oxidizes quinol molecules downstream of PSII and is required for adjusting the redox balance of the PQ pool (14, 15, 20, 59). The rate of quinol oxidation by PTOX was found to be relatively slow, only 5 e$^-$·s^{-1}·PSI^{-1} in Chlamydomonas (14), approximately fourfold slower than the rate of NADPH oxidation by FLVs (as calculated in this study). However, it was shown that stressed organisms that experience a highly reduced PQ pool accumulate high levels of PTOX proteins, which would facilitate PTOX-dependent reduction of O$_2$ to H$_2$O (19, 59–62). Here we show that PTOX may have a minor contribution to overall O$_2$ uptake when C6 cells (i.e., normal starch biosynthesis) are shifted from darkness to 300 μmol photons·m^{-2}·s^{-1} (Fig. 5). Nevertheless, inactivation of PTOX using PG led to an elevated reduction of the PQ pool for both C6 and *sta6* when the cells were maintained in the dark (Fig. 5*E*), which highlights the importance of PTOX in regulating the redox state of the PQ pool in

darkness. However, when starch synthesis was compromised (i.e., in *sta6* cells), the redox state of the PQ pool was highly elevated at all light intensities (Fig. 5*F*). Hence, we suggest that PTOX can become an important alternative outlet for electrons when various aspects of C metabolism/utilization, such as the storage of electrons in starch, are depressed.

Rerouting of electrons through alternative outlets allows photosynthetic organisms to cope with fluctuating environmental conditions. Here we show that Chlamydomonas activates various "sustainable" and "nonsustainable" electron transport pathways. The transient storage of fixed C, such as in starch, represents a sustainable sink for excitation energy; the energy is not lost but can be deployed for growth and maintenance when needed. However, under conditions in which CO$_2$ fixation and C storage are compromised and/or saturated, the cells can photochemically quench absorbed excitation energy through photoreduction of O$_2$, a nonsustainable outlet (the energetic electron can no longer be used as a source of energy) in which photosynthetically generated electrons are used for the catalytic reduction of O$_2$ to H$_2$O; FLV and PTOX can both catalyze this reaction. While photosynthetic reaction centers and electron transport components provide reducing equivalents that fuel C metabolism, FLVs appear to function as a clutch, dissipating excess energy stored in the electron transport system when the CBBC has not been fully "switched on," suggesting potential regulatory interactions between CBBC proteins/metabolites and FLV activity. However, synthesis of starch acts as a battery that is being charged and prevents feedback inhibition of CBBC enzymes by phosphorylated CBBC sugars; the energy stored as starch can be used when needed through catabolic reactions that release reductant, ATP, and C backbones. Finally, PTOX proteins are sensitive to redox changes associated with the PQ pool, which can be triggered by limitations in electron utilization by downstream reactions. As the redox state of the PET chain increases and a greater proportion of the PQ pool becomes reduced, PTOX acts like a valve on a pressure cooker, facilitating the routing of "overflow" electrons to the reduction of O$_2$. PTOX enables continued functioning of PSII in generating a charge separation and driving H$_2$O oxidation, while at the same time limiting photodamage. Previous studies have also provided supportive evidence for the recruitment of alternative, nonsustainable electron outlets when CBBC is not functioning, including the routing of electrons toward Mehler reactions and mitochondrial respiration (29, 63), or toward H$_2$ production when the cells are under anoxic conditions (22).

Future challenges in optimizing photosynthetic outputs will likely be facilitated by elucidating the regulation of enzymes involved in both sustainable and nonsustainable photochemical quenching. However, we still do not fully understand the mechanisms underlying the transitions between storing/assimilating and dissipating excitation energy when CBBC cannot properly utilize the energy generated by PET. A regulatory mechanism for controlling PET and the production ATP and

NADPH based on the status of downstream electron sinks, and that is still not well understood, has been designated "photosynthetic control" (64). Such control potentially involves the redox conditions and ferredoxin-thioredoxin control, the thylakoid membrane proton motif force, changes in the rate of CEF, and accumulation of specific metabolites associated with the CBBC. Further information concerning these processes can be exploited to develop platforms for engineering the energetics of plants for better satisfying global food and resource needs.

Materials and Methods

Strains and Cell Growth. The *sta6* mutant (CC-4348; *sta6*[−]; *rbo1*[−]) and the genetically complemented *sta6::STA6* strain, designated C6 (CC-4567) (42) were maintained at ~10 μmol photons·m^{-2}·s^{-1} on solid Tris-acetate-phosphate (TAP) medium (65). Cells were inoculated from solid TAP into liquid TAP medium and grown in flasks at ~40 μmol photons·m^{-2}·s^{-1} (aerated by shaking at ~150 rpm) to midlogarithmic phase (~1 × 10^6 cells·mL^{-1}). The volume of cell culture containing 60 μg of Chl was pelleted by centrifugation [1,000 × *g*, 4 min, room temperature (RT)], washed twice with fresh photoautotrophic Mops-Tris medium (20 mM Mops titrated with Tris base powder to pH 7.5, 0.2 g·L^{-1} K$_2$HPO$_4$, 0.11g·L^{-1} KH$_2$PO$_4$, 50 mg·L^{-1} CaCl$_2$, 100 mg·L^{-1} MgSO$_4$, 37.5 mg·L^{-1} NH$_4$Cl, and 1:1,000 Hutner trace elements) (modified from ref. 66) and resuspended in the same medium to a final Chl concentration of 2 to 4 μg·mL^{-1} (~60 mL of medium). These cultures were bubbled with 2% CO$_2$ in glass tubes and grown at 100 μmol photons·m^{-2}·s^{-1} (white light) to a final concentration of 10 to 15 μg Chl·mL^{-1}.

Chl Concentration. Chl concentrations were determined from methanol-extracted pigments according to ref. 67. Briefly, cells were pelleted by centrifugation (13,000 × *g*, 2 min, RT) and resuspended in 100% methanol. Cell debris from methanol extracted samples was pelleted (13,000 × *g*, 5 min, RT) and the supernatant containing the pigments was transferred to plastic cuvettes. Total Chl was calculated according to the equation Chl = 22.12 × *A*652 + 2.71 × *A*665, where *A*652 and *A*665 are absorbances at 652 and 665 nm, respectively.

Dark Respiration. Dark respiration at different light intensities was measured using a Pt-Ag/AgCl polarographic electrode system (ALGI) equipped with a temperature-controlled, 1-mL glass water-jacketed reaction chamber, two YSI 5331A electrodes (Yellow Springs Instruments) polarized at −0.8 V, and an atmospheric barometric pressure sensor (Infineon Technologies Americas Corp.). Assays were performed using 1.5 mL of actively growing cells that were purged with 1% CO$_2$/99% He supplemented with 12 μL of 0.5 M potassium bicarbonate in 5 mM Tris. After injection into the reaction chamber, the rate of change in O$_2$ levels was measured sequentially at light intensities of 40, 80, 160, 320, 640, 1,280, and 1,600 μmol photons·m^{-2}·s^{-1} (photosynthetic active radiation, PAR) (Luxeon III Star; Lumileds); each intensity was maintained for 3 min followed by a 3-min intervening dark period and then the light level was raised to the next higher intensity (stepped change) until the full range of intensities was tested. Before the measurement of each experimental series, the electrodes were calibrated with air (~21% oxygen) and with 1% CO$_2$/99% He purged Mops medium (0% oxygen). The intensity of light from the LEDs was calibrated using a Walz US-SQS/L spherical microquantum sensor.

Chl Fluorescence Analysis. Chl fluorescence was measured using a DUAL-PAM-100 fluorometer. For monitoring Chl fluorescence at different light intensities (i.e., a light curve), the cells were supplemented with 2 mM NaHCO$_3$ and exposed to increasing light intensities for 1 min at each intensity. The quantum efficiency of PSII as well as photochemical quenching, qL [and accordingly 1-qL (50)] were directly calculated from the light curves.

O$_2$ Production and Light-Driven O$_2$ Photoreduction. In vivo ^{16}O$_2$ photoproduction rates and ^{18}O$_2$ uptake rates were determined using a custom-built MIMS with a Pfeiffer quadrupole PrismaPlus QME-220 (Pfeiffer Vacuum) coupled with a Pt-Ag/AgCl polarographic electrode system (ALGI) equipped with a temperature-controlled, water-jacketed 1-mL glass cell, a YSI 5331A electrode (Yellow Springs Instruments) polarized at −0.8 V, and an atmospheric barometric pressure sensor (Infineon Technologies Americas Corp.). For performing MIMS assays, 1.5 mL of actively growing cells were purged with 1% CO$_2$/99% He that was spiked with 0.5 mL 99% ^{18}O$_2$ and supple-

mented with 4 mM potassium bicarbonate that was suspended in fresh medium. After injection of the sample into the reaction chamber, a light regime (Luxeon III Star; Lumileds) was applied as follows: 5 min of dark, 6 min of light, and then 3 min of dark. The light intensities used for these experiments were 50, 150, 300, and 1,000 μmol photons·m^{-2}·s^{-1} (a single intensity of light was used for each experiment). The electrode and MIMS were calibrated before each measurement using atmospherically equilibrated medium, 1% CO$_2$/He balance purged medium and purged medium spiked with 0.5 mL 99% ^{18}O$_2$. The light intensity from the LED was calibrated using a Walz US-SQS/L spherical micro quantum sensor. Gross O$_2$ production and net uptake were calculated according to the following equations (68).

$$\Delta \text{Gross } O_2 \text{uptake} = \Delta^{18}O_2 * \left(1 + \left[^{16}O_2\right]/\left[^{18}O_2\right]\right)$$

$$\Delta \text{Gross } O_2 \text{production} = \Delta^{16}O_2 - \Delta^{18}O_2 * \left(\left[^{16}O_2\right]/\left[^{18}O_2\right]\right)$$

$$\Delta \text{Net } O_2 \text{ production} = \Delta \text{gross } O_2 \text{ production} - \Delta \text{gross } O_2 \text{ uptake.}$$

To inhibit alternative oxidases, samples were supplemented with 2 mM *n*-propyl gallate (Sigma) suspended in ethanol.

Untargeted Metabolite Profiling. Cells (1 × 10^7 per mL) were pelleted (3,000 × *g* × 4 min, RT) and resuspended in a glass beaker with MOP-Tris medium, pH 7.5, supplemented with 4 mM bicarbonate. Cells were dark acclimated for 5 min with continued stirring. Cells (1 mL) were collected at the end of the dark period and at different times after the light was switched on (300 μmol photons·m^{-2}· s^{-1}; 10, 20, 30, 60, 120, and 300 s). To quench cellular metabolism, each sample was quickly transferred into a 2-mL tube containing 1 mL of quenching solution (70% methanol incubated at 80 °C and maintained on dry ice); the cells maintained on dry ice remained unfrozen. After collecting all time points, the cells were pelleted by centrifugation in a microfuge (30 s at maximal speed, 1 °C) and the pellets quickly frozen in liquid nitrogen and kept at −80 °C until analysis.

Frozen cell pellets were lyophilized for 4 h using a Labconco Freezone freeze dry system (Labconco Corp.), and 1 mL 10:3:1 chloroform/methanol/water was added. The resulting solution was homogenized by 2 min of shaking and then centrifuged for 2 min at 15,000 × *g*. After centrifugal separation, the supernatant was transferred to a clean 1.5-mL Eppendorf tube and dried. Five microliters of methoxyamine hydrochloride (40 mg·mL^{-1} in pyridine) was added to the dried extract and incubated (while shaking) for 1.5 h at 30 °C. Following the incubation period, 45 μL *N*-methyl-*N*-(trimethylsilyl) trifluoroacetamide were added and the extract were incubated (while shaking) for 30 min at 37 °C. The resulting solution was transferred to a clean crimp-top autosampler vial with insert and analyzed using a LECO Pegasus BT GC-TOF system (LECO Corp.). For chromatographic separation, an Rtx-5Sil MS column (30 m, 0.25 μm × 0.25 mm i.d.; Restek Corp.) was used with helium carrier gas (99.9999%; Airgas) at a constant flow rate of 1 mL·min^{-1}. The inlet temperature was maintained at 275 °C, with an injection volume of 0.5 μL. The oven temperature started at 50 °C, held for 1 min, and then ramped to 330 °C at a rate of 20 °C·min^{-1} and held constant for 5 min. The mass spectrometer was operated in electron ionization mode at 70 eV with a source temperature of 250 °C and transfer line temperature of 280 °C. Spectra were acquired at 17 spectra per s over 85- to 500-Da mass range. For quantification of selected analytes, standard solutions were prepared in methanol and dried down using the same procedure described above. The resulting data were processed using BinBase mass spectral database (69)

Data Analyses. The gas exchange data were analyzed (statistics, data filtering, and curve fitting) using Origin 2017. Basal rates of O$_2$ uptake were calculated as follows: O$_2$ uptake data derived from the late light period (500 to 630 s from the onset of light; *SI Appendix*, Fig. S4A) was fitted to a linear curve [*y* = *ax* + *b*] and the average rate of O$_2$ uptake over this period was calculated.

1. B. B. Buchanan, The path to thioredoxin and redox regulation in chloroplasts. *Annu. Rev. Plant Biol.* **67**, 1–24 (2016).
2. L. Michelet *et al.*, Redox regulation of the Calvin-Benson cycle: Something old, something new. *Front. Plant Sci.* **4**, 470 (2013).
3. W. Wirtz, M. Stitt, H. W. Heldt, Light activation of Calvin cycle enzymes as measured in pea leaves. *FEBS Lett.* **142**, 223–226 (1982).
4. K. Asada, The water-water cycle in chloroplasts: Scavenging of active oxygens and dissipation of excess photons. *Annu. Rev. Plant Physiol. Plant Mol. Biol.* **50**, 601–639 (1999).
5. G. Curien *et al.*, The water to water cycles in microalgae. *Plant Cell Physiol.* **57**, 1354–1363 (2016).
6. A. H. Mehler, Studies on reactions of illuminated chloroplasts. I. Mechanism of the reduction of oxygen and other Hill reagents. *Arch. Biochem. Biophys.* **33**, 65–77 (1951).
7. A. H. Mehler, A. H. Brown, Studies on reactions of illuminated chloroplasts. III. Simultaneous photoproduction and consumption of oxygen studied with oxygen isotopes. *Arch. Biochem. Biophys.* **38**, 365–370 (1952).
8. F. Chaux *et al.*, Flavodiiron proteins promote fast and transient O_2 photoreduction in Chlamydomonas. *Plant Physiol.* **174**, 1825–1836 (2017).
9. Y. Helman *et al.*, Genes encoding A-type flavoproteins are essential for photoreduction of O_2 in cyanobacteria. *Curr. Biol.* **13**, 230–235 (2003).
10. Y. Allahverdiyeva *et al.*, Flavodiiron proteins Flv1 and Flv3 enable cyanobacterial growth and photosynthesis under fluctuating light. *Proc. Natl. Acad. Sci. U.S.A.* **110**, 4111–4116 (2013).
11. C. Gerotto *et al.*, Flavodiiron proteins act as safety valve for electrons in *Physcomitrella patens*. *Proc. Natl. Acad. Sci. U.S.A.* **113**, 12322–12327 (2016).
12. K.-V. Dang *et al.*, Combined increases in mitochondrial cooperation and oxygen photoreduction compensate for deficiency in cyclic electron flow in *Chlamydomonas reinhardtii*. *Plant Cell* **26**, 3036–3050 (2014).
13. G. Peltier, L. Cournac, Chlororespiration. *Annu. Rev. Plant Biol.* **53**, 523–550 (2002).
14. L. Houille-Vernes, F. Rappaport, F.-A. Wollman, J. Alric, X. Johnson, Plastid terminal oxidase 2 (PTOX2) is the major oxidase involved in chlororespiration in Chlamydomonas. *Proc. Natl. Acad. Sci. U.S.A.* **108**, 20820–20825 (2011).
15. W. J. Nawrocki, N. J. Tourasse, A. Taly, F. Rappaport, F.-A. Wollman, The plastid terminal oxidase: Its elusive function points to multiple contributions to plastid physiology. *Annu. Rev. Plant Biol.* **66**, 49–74 (2015).
16. F. Jans *et al.*, A type II NAD(P)H dehydrogenase mediates light-independent plastoquinone reduction in the chloroplast of Chlamydomonas. *Proc. Natl. Acad. Sci. U.S.A.* **105**, 20546–20551 (2008).
17. C. Desplats *et al.*, Characterization of Nda2, a plastoquinone-reducing type II NAD(P)H dehydrogenase in chlamydomonas chloroplasts. *J. Biol. Chem.* **284**, 4148–4157 (2009).
18. G. Peltier, E. M. Aro, T. Shikanai, NDH-1 and NDH-2 plastoquinone reductases in oxygenic photosynthesis. *Annu. Rev. Plant Biol.* **67**, 55–80 (2016).
19. S. I. Saroussi, T. M. Wittkopp, A. R. Grossman, The type II NADPH dehydrogenase facilitates cyclic electron flow, energy-dependent quenching, and chlororespiratory metabolism during acclimation of *Chlamydomonas reinhardtii* to nitrogen deprivation. *Plant Physiol.* **170**, 1975–1988 (2016).
20. A. Krieger-Liszkay, K. Feilke, The dual role of the plastid terminal oxidase PTOX: Between a protective and a pro-oxidant function. *Front. Plant Sci.* **6**, 1147 (2016).
21. C. Peterhansel *et al.*, Photorespiration. *Arabidopsis Book* **8**, e0130 (2010).
22. E. S. Bamberger, D. King, D. L. Erbes, M. Gibbs, H_2 and CO_2 Evolution by anaerobically adapted *Chlamydomonas reinhardtii* F-60. *Plant Physiol.* **69**, 1268–1273 (1982).
23. A. Hemschemeier, T. Happe, Alternative photosynthetic electron transport pathways during anaerobiosis in the green alga *Chlamydomonas reinhardtii*. *Biochim. Biophys. Acta* **1807**, 919–926 (2011).
24. J. Alric, X. Johnson, Alternative electron transport pathways in photosynthesis: A confluence of regulation. *Curr. Opin. Plant Biol.* **37**, 78–86 (2017).
25. X. Johnson, J. Alric, Central carbon metabolism and electron transport in *Chlamydomonas reinhardtii*: Metabolic constraints for carbon partitioning between oil and starch. *Eukaryot. Cell* **12**, 776–793 (2013).
26. R. Scheibe, Malate valves to balance cellular energy supply. *Physiol. Plant.* **120**, 21–26 (2004).
27. K. Yoshida, I. Terashima, K. Noguchi, Up-regulation of mitochondrial alternative oxidase concomitant with chloroplast over-reduction by excess light. *Plant Cell Physiol.* **48**, 606–614 (2007).
28. B. Bailleul *et al.*, Energetic coupling between plastids and mitochondria drives CO_2 assimilation in diatoms. *Nature* **524**, 366–369 (2015).
29. X. Johnson *et al.*, Proton gradient regulation 5-mediated cyclic electron flow under ATP- or redox-limited conditions: A study of ΔATpase *pgr5* and Δ*rbcL pgr5* mutants in the green alga *Chlamydomonas reinhardtii*. *Plant Physiol.* **165**, 438–452 (2014).
30. G. Noctor, C. Dutilleul, R. De Paepe, C. H. Foyer, Use of mitochondrial electron transport mutants to evaluate the effects of redox state on photosynthesis, stress tolerance and the integration of carbon/nitrogen metabolism. *J. Exp. Bot.* **55**, 49–57 (2004).
31. S. C. Zeeman, J. Kossmann, A. M. Smith, Starch: Its metabolism, evolution, and biotechnological modification in plants. *Annu. Rev. Plant Biol.* **61**, 209–234 (2010).
32. P. Geigenberger, Regulation of starch biosynthesis in response to a fluctuating environment. *Plant Physiol.* **155**, 1566–1577 (2011).
33. P. L. Keeling, A. M. Myers, Biochemistry and genetics of starch synthesis. *Annu. Rev. Food Sci. Technol.* **1**, 271–303 (2010).
34. B. Pfister, S. C. Zeeman, Formation of starch in plant cells. *Cell. Mol. Life Sci.* **73**, 2781–2807 (2016).
35. M. Siaut *et al.*, Oil accumulation in the model green alga *Chlamydomonas reinhardtii*: Characterization, variability between common laboratory strains and relationship with starch reserves. *BMC Biotechnol.* **11**, 7 (2011).
36. M. P. Davey *et al.*, Triacylglyceride production and autophagous responses in *Chlamydomonas reinhardtii* depend on resource allocation and carbon source. *Eukaryot. Cell* **13**, 392–400 (2014).
37. S. Saroussi, E. Sanz-Luque, R. G. Kim, A. R. Grossman, Nutrient scavenging and energy management: Acclimation responses in nitrogen and sulfur deprived Chlamydomonas. *Curr. Opin. Plant Biol.* **39**, 114–122 (2017).
38. S. G. Ball, P. Deschamps, "Starch metabolism" in *The Chlamydomonas Sourcebook*, E. H. Harris, D. B. Stern, G. B. Witman, Eds. (Elsevier, 2009), pp. 1–40.
39. C. Zabawinski *et al.*, Starchless mutants of *Chlamydomonas reinhardtii* lack the small subunit of a heterotetrameric ADP-glucose pyrophosphorylase. *J. Bacteriol.* **183**, 1069–1077 (2001).
40. A. Krishnan *et al.*, Metabolic and photosynthetic consequences of blocking starch biosynthesis in the green alga *Chlamydomonas reinhardtii sta6* mutant. *Plant J.* **81**, 947–960 (2015).
41. J. Sun, T. W. Okita, G. E. Edwards, Modification of carbon partitioning, photosynthetic capacity, and O_2 sensitivity in Arabidopsis plants with low ADP-glucose pyrophosphorylase activity. *Plant Physiol.* **119**, 267–276 (1999).
42. Y. Li *et al.*, Chlamydomonas starchless mutant defective in ADP-glucose pyrophosphorylase hyper-accumulates triacylglycerol. *Metab. Eng.* **12**, 387–391 (2010).
43. I. K. Blaby *et al.*, Systems-level analysis of nitrogen starvation-induced modifications of carbon metabolism in a *Chlamydomonas reinhardtii* starchless mutant. *Plant Cell* **25**, 4305–4323 (2013).
44. S. Schmollinger *et al.*, Nitrogen-sparing mechanisms in Chlamydomonas affect the transcriptome, the proteome, and photosynthetic metabolism. *Plant Cell* **26**, 1410–1435 (2014).
45. A. Anderson *et al.*, Exploiting algal NADPH oxidase for biophotovoltaic energy. *Plant Biotechnol. J.* **14**, 22–28 (2016).
46. G. Shimakawa *et al.*, The Liverwort, Marchantia, drives alternative electron flow using a flavodiiron protein to protect PSI. *Plant Physiol.* **173**, 1636–1647 (2017).
47. V. Lysenco, Y. Guo, O. Chugueva, Cyclic electron transport around photosystem II: Mechanisms and methods of study. *Am. J. Plant Physiol.* **12**, 1–9 (2017).
48. K. Suzuki, T. G. Mamedov, T. Ikawa, A mutant of *Chlamydomonas reinhardtii* with reduced rate of photorespiration. *Plant Cell Physiol.* **40**, 792–799 (1999).
49. M. Trouillard *et al.*, Kinetic properties and physiological role of the plastoquinone terminal oxidase (PTOX) in a vascular plant. *Biochim. Biophys. Acta* **1817**, 2140–2148 (2012).
50. D. M. Kramer, G. Johnson, O. Kiirats, G. E. Edwards, New fluorescence parameters for the determination of QA redox state and excitation energy fluxes. *Photosynth. Res.* **79**, 209 (2004).
51. P. G. Falkowski, Y. Fujita, A. Ley, D. Mauzerall, Evidence for cyclic electron flow around Photosystem II in *Chlorella pyrenoidosa*. *Plant Physiol.* **81**, 310–312 (1986).
52. O. Prasil, Z. Kolber, J. A. Berry, P. G. Falkowski, Cyclic electron flow around Photosystem II in vivo. *Photosynth. Res.* **48**, 395–410 (1996).
53. W. Onno Feikema, M. A. Marosvölgyi, J. Lavaud, H. J. van Gorkom, Cyclic electron transfer in photosystem II in the marine diatom *Phaeodactylum tricornutum*. *Biochim. Biophys. Acta* **1757**, 829–834 (2006).
54. H. Yamamoto, S. Takahashi, M. R. Badger, T. Shikanai, Artificial remodelling of alternative electron flow by flavodiiron proteins in Arabidopsis. *Nat. Plants* **2**, 16012 (2016).
55. G. DalCorso *et al.*, A complex containing PGRL1 and PGR5 is involved in the switch between linear and cyclic electron flow in Arabidopsis. *Cell* **132**, 273–285 (2008).
56. X. Johnson, J. Alric, Interaction between starch breakdown, acetate assimilation, and photosynthetic cyclic electron flow in *Chlamydomonas reinhardtii*. *J. Biol. Chem.* **287**, 26445–26452 (2012).
57. J. A. Bassham, Photosynthetic carbon metabolism. *Proc. Natl. Acad. Sci. U.S.A.* **68**, 2877–2882 (1971).
58. L. Marri *et al.*, Prompt and easy activation by specific thioredoxins of calvin cycle enzymes of *Arabidopsis thaliana* associated in the GAPDH/CP12/PRK supramolecular complex. *Mol. Plant* **2**, 259–269 (2009).
59. S. Bailey *et al.*, Alternative photosynthetic electron flow to oxygen in marine *Synechococcus*. *Biochim. Biophys. Acta* **1777**, 269–276 (2008).
60. C. Laureau *et al.*, Plastid terminal oxidase (PTOX) has the potential to act as a safety valve for excess excitation energy in the alpine plant species Ranunculus glacialis L. *Plant Cell Environ.* **36**, 1296–1310 (2013).
61. M. J. Quiles, Stimulation of chlororespiration by heat and high light intensity in oat plants. *Plant Cell Environ.* **29**, 1463–1470 (2006).
62. P. Stepien, G. N. Johnson, Contrasting responses of photosynthesis to salt stress in the glycophyte Arabidopsis and the halophyte thellungiella: Role of the plastid terminal oxidase as an alternative electron sink. *Plant Physiol.* **149**, 1154–1165 (2009).
63. R. J. Radmer, B. Kok, Photoreduction of O_2 primes and replaces CO_2 assimilation. *Plant Physiol.* **58**, 336–340 (1976).
64. C. Foyer, R. Furbank, J. Harbinson, P. Horton, The mechanisms contributing to photosynthetic control of electron transport by carbon assimilation in leaves. *Photosynth. Res.* **25**, 83–100 (1990).
65. E. H. Harris, D. B. Stern, G. B. Witman, Eds. *The Chlamydomonas Sourcebook* (Academic Press, London, ed. 2, 2009).
66. A. M. Geraghty, J. C. Anderson, M. H. Spalding, A 36 kilodalton limiting-CO_2 induced polypeptide of Chlamydomonas is distinct from the 37 kilodalton periplasmic carbonic anhydrase 1. *Plant Physiol.* **93**, 116–121 (1990).
67. R. J. Porra, W. A. Thompson, P. E. Kriedemann, Determination of accurate extinction coefficients and simultaneous equations for assaying chlorophylls a and b extracted with four different solvents: Verification of the concentration of chlorophyll standards by atomic absorption spectroscopy. *Biochim. Biophys. Acta* **975**, 384–394 (1989).
68. K. Beckmann, J. Messinger, M. R. Badger, T. Wydrzynski, W. Hillier, On-line mass spectrometry: Membrane inlet sampling. *Photosynth. Res.* **102**, 511–522 (2009).
69. O. Fiehn, G. Wohlgemuth, M. Scholz, "Setup and annotation of metabolomic experiments by integrating biological and mass spectrometric metadata" in *Data Integration in the Life Sciences*, B. Ludäscher, L. Raschid, Eds., Lecture Notes in Computer Science (Springer, Berlin, 2005), pp. 224–239.

PLANT BIOLOGY